Survey of four material models for ballistic simulations of high-strength concrete

Andria Antoniou[1,2], Martin Kristoffersen[1,2], Tore Børvik [1,2]

[1]Structural Impact Laboratory (SIMLab), Department of Structural Engineering, NTNU – Norwegian University of Science and Technology, NO-7491 Trondheim, Norway
[2]Centre for Advanced Structural Analysis (CASA), NTNU, NO-7491 Trondheim, Norway

Abstract

*This study briefly presents four concrete models used for ballistic impact simulations. The models are the RHT model (***MAT_272** or ***MAT_RHT**), the CSCM model (***MAT_159** or ***MAT_CSCM**), the K&C model (***MAT_072R3** or ***MAT_CONCRETE_DAMAGE_REL3**) and a modified Holmquist-Jonson-Cook model (MHJC). The first three are available as standard models in LS-DYNA with the option to automatically generate their constitutive parameters. The MHJC model has been implemented as a user subroutine. In the present study, we calibrated the MHJC model parameters for C75 high-strength concrete by using laboratory material experiments and data from the literature. Ballistic simulations of C75 concrete slabs impacted by ogival projectiles validated the accuracy of the calibrated parameters. We evaluated the default parameter generation of the former three models compared to the latter.*

Keywords: ballistic simulations, high strength concrete, concrete models, MHJC, RHT, CSCM, K&C

1 Introduction

The protection of critical infrastructure against ballistic impact scenarios is crucial for the safety of the public. Shielding barriers are commonly made of concrete and their design poses significant challenges. Accurate numerical models of concrete are in great demand especially for conditions involving high stain rates, high triaxial pressures and complicated fracture modes. Today, finite element (FE) constitutive models are extensively used to address the problem. All the while, accurate material data reflecting concrete behaviour under such conditions is rare and difficult to produce.

Three of the most commonly used concrete models are (1) ***MAT_272** (***MAT_RHT**) or the Riedel-Hiermaier-Thoma (RHT) model [1], (2) ***MAT_159** (***MAT_CSCM**) or the continuous surface cap model (CSCM) [2] and (3) ***MAT_072R3** (***MAT_CONCRETE_DAMAGE_REL3**) or the Karagozian and Case (K&C) model – Release III [3]. These are standard models available in LS-DYNA with the optional setting for automated generation of material parameters. A thorough calibration of these models can be challenging because of their numerous parameters. Further, a modified version of the Holmquist-Johnson-Cook (MHJC) model [4] has been implemented in LS-DYNA as a user subroutine and was included because of its comparatively convenient parameter calibration. Some differences and similarities between the models are identified in Section 2, while Section 3 contains simulations using these four concrete material models.

The main motivation behind the study is to investigate how well the automatically generated material cards predict the ballistic impact response of concrete slabs. For comparison, the somewhat simpler MHJC model calibrated to experimental data is included. In the current study, we considered a series of perforation experiments on high-strength concrete slabs with nominal unconfined compressive strength 75 MPa (C75) [5]. The slabs had a nominal thickness of 50 mm and were impacted by ogival-nosed projectiles made of hard steel. First, we identified the constitutive parameters of the MHJC model using material experiments (cylinder compression, cube compression and tensile splitting), data from the literature [6], and inverse modelling. Second, we simulated the perforation experiments with the obtained material parameters for the MHJC model. The numerical ballistic resistance was close to the experimental and thus verifies the accuracy of the calibrated MHJC model. Third, the automatically generated parameters were used to investigate their performance on the cylinder compression test. Fourth, we evaluated the automatic generation option for the parameter determination of the other three models (***MAT_272**, ***MAT_159** and ***MAT_072R3**) by comparing their ballistic response (in

terms of residual vs. initial velocity) with the MHJC simulations and the C75 perforation experiments from [5].

2 Concrete models

The concrete models RHT (***MAT_272**), CSCM (***MAT_159**), K&C - Release III (***MAT_072R3**) and MHJC consist of (1) elastic and plastic domains, (2) stress triaxiality and Lode dependency, (3) strain rate sensitivity, (4) pore collapse evolution and (5) damage accumulation.

The elastic regime of all four models is constrained by the yield surface. In stress space the yield surface has a certain degree of symmetry around the hydrostatic axis. Therefore, the yield surface depends on the equivalent shear stress which is the radial distance from the hydrostatic axis. The hydrostatic pressure P is characterized by the first invariant I_1 of the stress tensor $\boldsymbol{\sigma}$.

$$P = \frac{I_1}{3} = \frac{1}{3}\mathrm{tr}(\boldsymbol{\sigma}) \tag{1}$$

The equivalent shear stress q is related to the second deviatoric invariant J_2 of the stress deviator tensor $\mathbf{s}$,

$$q = \sqrt{3\,J_2} = \sqrt{{}^3\!/_2\,\mathrm{tr}(\mathbf{s^2})} \tag{2}$$

The compression yield surface in the meridian plane can be expressed as a function of P and q,

$$\mathcal{F}_y = f(P, q) \tag{3}$$

The stress triaxiality is introduced by a reduction factor $\mathcal{R}$. The reduction factor depends on the Lode angle θ, which is a function of the equivalent shear stress q and the third deviatoric invariant $J_3 = |\,\mathbf{s}\,|$,

$$\theta = \frac{1}{3}\arccos\left(\frac{27J_3}{2q^3}\right) \tag{4}$$

The Lode angle denotes the position of the stress state in the deviatoric plane. Thus, the reduction factor expresses the elastic limit of any stress state relative to the compression meridian yield surface. Hence, the general form of yield surface in the stress space is

$$\mathcal{F}_y = f(P, q, \theta) \tag{5}$$

The reduction factor $\mathcal{R}$ follows the Rubin model expression [7] for the CSCM model while the Willam-Warnke model expression [8] (a subset of the Rubin model) is employed for the MHJC, RHT and K&C models. The expressions permit a smooth transition in the deviatoric plane from a triangular shape with smooth corners at low pressures to a circular shape at high pressures.

However, the strain-rate sensitivity is introduced with a different expression for each model. A power equation increases the yield strength of the MHJC model multiplicatively as a function of the equivalent deviatoric strain rate $\dot{\varepsilon}_{\mathrm{eq}}$

$$F_{\mathrm{rate}} = \left(1 + \frac{\dot{\varepsilon}_{\mathrm{eq}}}{\dot{\varepsilon}_0}\right)^C \tag{6}$$

where $\dot{\varepsilon}_0$ is the reference strain rate and C is the strain-rate sensitivity exponent.

The strength of the CSCM model increases with increasing strain rate with a viscoplastic algorithm which interpolates between the trial elastic stress σ_{ij}^{T} and the plastic response without rate effects σ_{ij}^{p}.

$$\sigma_{ij}^{\mathrm{vp}} = (1-\gamma)\sigma_{ij}^{\mathrm{T}} + \gamma\sigma_{ij}^{\mathrm{p}} \quad \text{with} \quad \gamma = \frac{\Delta t/\eta}{1 + \Delta t/\eta} \tag{7}$$

The interpolation is controlled by the parameter γ which is dependent on the time step Δt and includes a fluidity coefficient η which is computed internally by a set of user-provided fluidity coefficients $\eta_{\mathrm{s}}, \eta_{\mathrm{t}}$ and η_{c} in shear, tension, and compression, respectively.

The strain-rate dependence of the RHT model utilizes a power function nearly identical to the CEB model code [9] and is shown in Eq. (8), in which superscripts “c” and “t” denote compression and tension. Further, the different strain rates are the plastic strain rate $\dot{\varepsilon}_{\mathrm{p}}$, the reference strain rate $\dot{\varepsilon}_0{}^{\mathrm{c/t}}$, and the break strain rate $\dot{\varepsilon}_{\mathrm{p}}{}^{\mathrm{c/t}}$. $\beta^{\mathrm{c/t}}$ is the strain rate dependence exponent, and $\gamma^{\mathrm{c/t}}$ is calculated

internally from continuity requirements. Note that the strain-rate increase factor of RHT is entangled in the yield surface equation and it does not enhance the strength linearly. The expression for $F_{\text{rate}}^{\text{c/t}}$ is

$$F_{\text{rate}}^{\text{c/t}} = \begin{cases} \left(\dfrac{\dot{\varepsilon}_p}{\dot{\varepsilon}_0{}^{\text{c/t}}}\right)^{\beta^{\text{c/t}}}, & \dot{\varepsilon}_{\text{p}}{}^{\text{c/t}} \geq \dot{\varepsilon}_{\text{p}} \\ \gamma^{\text{c/t}}\sqrt[3]{\dot{\varepsilon}_{\text{p}}}, & \dot{\varepsilon}_{\text{p}} > \dot{\varepsilon}_{\text{p}}{}^{\text{c/t}} \end{cases} \tag{8}$$

The strain-rate enhancement of the K&C model is introduced on a tabulated form, or the automatic parameter generation option can induct the values from the CEB model code [9].

The pore collapse evolution for pure hydrostatic loading is described in terms of hydrostatic pressure – volumetric strain equations. The pressure-porosity constitutive model consists of three phases (1) fully elastic behaviour, (2) compaction; pores collapse with plastic deformation and (3) solidification; fully compacted. At the final phase the porosity is fully compressed, and the volumetric response returns elastic behaviour, although it retains the irreversible deformation from the second phase.

The pressure-porosity expression of the MHJC model constructs the three phases based on the volumetric strain μ limits (μ_{c} is the crush volumetric strain and μ_{l} the fully compacted volumetric strain),

$$P = \begin{cases} K_0\,\mu, & \mu \leq \mu_{\text{c}} \\ K_{\text{av}}\left(\mu - \mu_{\text{p}}\right), & \mu_{\text{c}} \leq \mu \leq \mu_{\text{l}} \\ K_1\,\overline{\mu} + K_2\,\overline{\mu}^2 + K_3\,\overline{\mu}^3, & \mu_{\text{l}} \leq \mu \end{cases} \tag{9}$$

The initial bulk modulus $K_0 = P_{\text{c}}/\mu_{\text{c}}$ and the average bulk modulus $K_{\text{av}} = K_0\left(1 - \frac{\mu_{\text{p}}}{\mu_{\text{l}}}\right) + K_1\frac{\mu_{\text{p}}}{\mu_{\text{l}}(1-\mu_{\text{l}})}$ are computed internally. Here, K_1 is the bulk modulus at the end of the compaction phase and corresponds to the solidification pressure P_{l} where P_{c} is the crush pressure. Note that K_{av} ranges between K_0 and K_1 depending on the plastic volumetric strain μ_{p}. The solidification phase is governed by a cubic function depending on $\overline{\mu} = (\mu - \mu_{\text{l}})/(1 + \mu_{\text{l}})$ where K_1, K_2 and K_3 are the solidification function coefficients.

The plastic volumetric strain μ_{p} of the CSCM model is controlled by the expression in Eq. (10), where w is the fully compacted plastic volumetric strain, D_1 and D_2 are shape factors of the pressure-volumetric strain curve and X_d denotes the crush pressure limit. The elastic pressure limit is defined by a cap function $X(\kappa)$ and the pressure is computed with the aforementioned viscoplastic algorithm in Eq. (7). Bear in mind that the CSCM model does not comprise any alteration of the bulk modulus.

$$\mu_{\text{p}} = w\left[1 - e^{-D_1[X(\kappa)-X_d]-D_2[X(\kappa)-X_d]^2}\right] \tag{10}$$

The pressure-porosity expression of the RHT model is quite similar to the MHJC expression. Two major differences are: (1) the pre-consolidation pressure $P_{\text{c}}(\alpha)$ is strongly dependent on the porosity history variable α, the initial porosity α_0, and the porosity exponent N, (2) the bulk modulus is constant throughout the elastic and the compaction phases. Likewise, P_{el} is the crush pressure and P_{co} is the solidification pressure.

$$P_{\text{c}}(a) = P_{\text{co}} - (P_{\text{co}} - P_{\text{el}})\left(\frac{\alpha - 1}{\alpha_0 - 1}\right)^{1/N} \tag{11}$$

An input equation of state (EoS) in tabulated form characterizes the hydrostatic pressure – volumetric strain behaviour of the K&C model.

The damage formulations of the four models under investigation have not been evaluated in the present study. For a more detailed description of the models, the readers are referred to [1] for RHT, [2] for CSCM, [3] and [10] for K&C and [4] for MHJC.

3 Evaluation of concrete models

The main objectives of this study are to highlight some differences between the chosen material models as done in Section 2, and to evaluate the default parameter generation option of ***MAT_272**, ***MAT_159** and ***MAT_072R3** for perforation simulations. Indeed, a detailed calibration of these models is challenging because of their numerous parameters. Therefore, the numerical responses of the three models (RHT, CSCM, and K&C) are compared with a modified version of the Holmquist-Johnson-Cook (MHJC) model [4] for which a simplified calibration is performed based on the data in Table 1 and the experimentally obtained engineering stress-strain curve in Fig. 1 (left). The MHJC model is chosen because it contains a comparatively short list of constitutive parameters and is thus easier to calibrate given a standard set of concrete tests.

Both the concrete composition and the mechanical properties of the C75 concrete are listed in Table 1. The mechanical properties were obtained experimentally through cylinder compression tests, cube compression tests and tensile splitting tests. This concrete mix was used to cast slabs with dimensions $625 \times 625 \times 50$ mm^3. The slabs were used in perforations tests with impact velocities ranging from 140 m/s to 300 m/s. Both the impact velocities v_i and the residual velocities v_r were measured by high-speed cameras. Ogival-nosed projectiles with diameter $d_\mathrm{p} = 20$ mm, length $l_\mathrm{p} = 98$ mm, mass $m_\mathrm{p} = 196$ g and critical-radius-head $\mathrm{CRH} = 3$ were used for the perforation tests. The experimental results in terms of residual velocity vs. impact velocity were used as a basis for comparison with the simulations. All experiments were conducted at SIMLab and are detailed in [5].

Composition		**Mechanical properties**	
Cement (kg/m^3)	427	Compressive strength (MPa)	75
Silica fume (kg/m^3)	48	Tensile strength (MPa)	5.2
Water (kg/m^3)	168	Slump (mm)	200
Fine aggregate: 0-8 mm (kg/m^3)	917	Density (kg/m^3)	2470
Coarse aggregate: 8-16 mm (kg/m^3)	881	Young's modulus E (GPa)	42
W/C ratio	0.39	Poisson's ratio ν	0.2

Table 1: Composition and mechanical properties of the C75 concrete.

3.1 MHJC parameter calibration

The calibration of the MHJC constitutive parameters is divided into (1) elastic behaviour, (2) quasi-static strength and yield surface, (3) pore collapse evolution and (4) strain-rate sensitivity. Note that this calibration procedure differs from the calibration based on digital image correlation in [5]. The shear modulus $G = E/[2(1+\nu)] = 17.5$ GPa and the initial bulk modulus $K_0 = E/[3(1-2\nu)] = 23.33$ GPa were calculated directly from the mechanical properties in Table 1.

The uniaxial compressive strength parameter $f_\mathrm{c} = 75$ MPa was introduced from the nominal value of the unconfined compression. On the other hand, the uniaxial tensile strength parameter $f_\mathrm{t} = 3.2$ MPa was identified by inverse modelling the tensile splitting test to obtain a peak stress of 5.2 MPa (Fig. 1 right). Next, the coefficients of the yield surface $B_\mathrm{c} = 1.62$ and $N_\mathrm{c} = 0.5$ were calibrated to satisfy the compressive peak stress in Fig. 1 (left). The Lode-dependent reduction factor $\mathcal{R}$ is computed internally. Fig. 2 (left) presents the yield surface of the compression meridian and Fig. 2 (right) the shape of the deviatoric plane from low to high hydrostatic pressure. Fig. 3 plots the factor of the tension and shear meridians.

A triaxial hydrostatic experiment is essential for the determination of the pore collapse evolution parameters. Triaxial hydrostatic experiments require high-capacity apparatus (GIGA press), and consequently the available experimental data are limited. For this reason, we estimated the pore collapse evolution parameters from Malecot et al. [6] and Magellanes et al. [10]. The pore collapse evolution parameters are the crush pressure $P_c = f_\mathrm{c}/3 = 25$ MPa, the solidification pressure

$P_l = 500$ MPa, the solidification bulk modulus $K_1 = 1.5\,K_0 = 35$ GPa, the crush volumetric strain $\mu_c = P_c/K_0 = 1.071 \cdot 10^{-3}$ and the fully compacted volumetric strain $\mu_l = 0.057714$. Further, the solidification coefficients K_1 and K_2 were set equal to zero for simplicity, thus reducing the solidification phase of Eq. (9) to a linear function. The hydrostatic test simulation is given in Fig. 4 (left), in which the slope of the first branch implies to (K_0) and the slope of the third branch to (K_1).

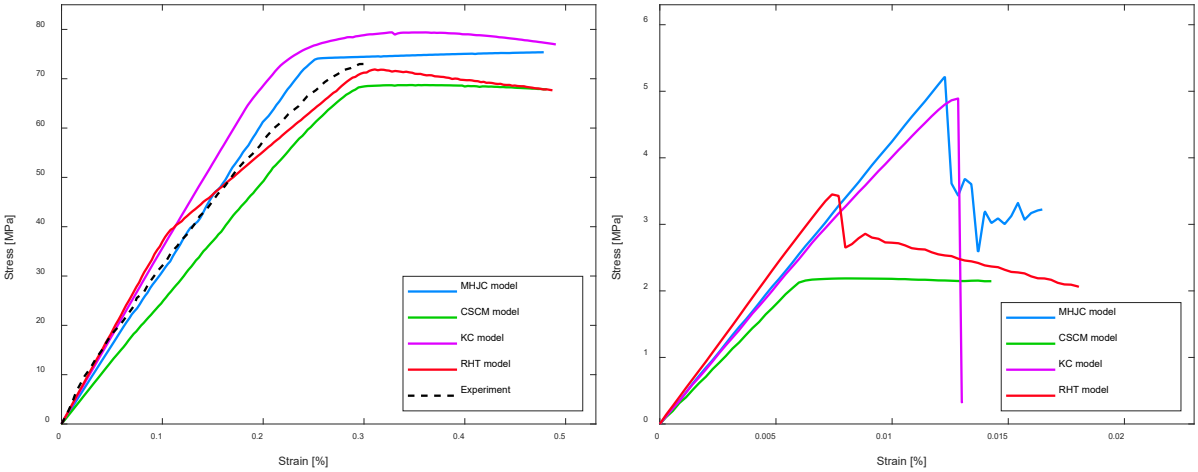

Fig. 1: Stress-strain curves of quasi-static compression (left) and tension (right)

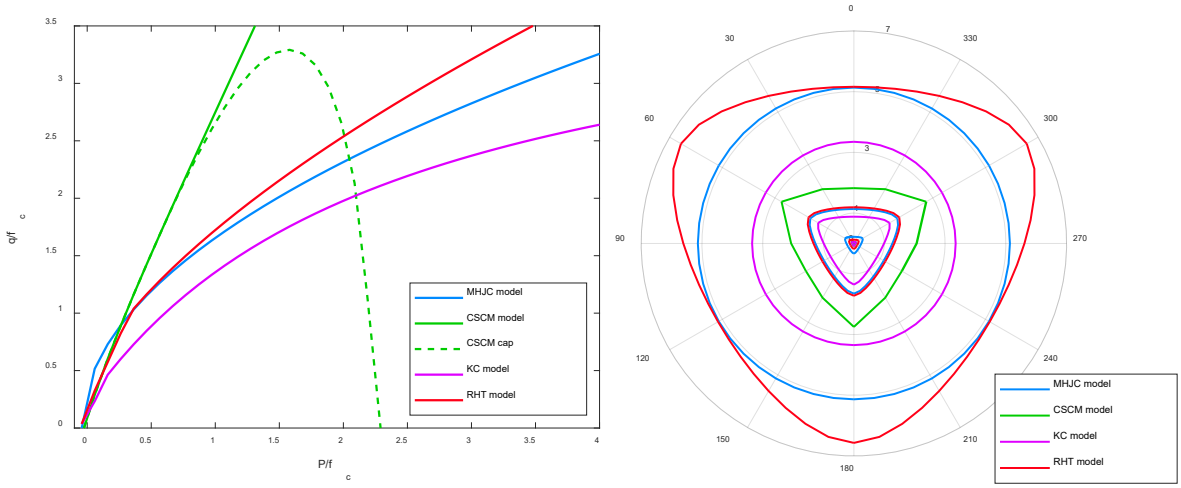

Fig. 2: Compression meridian yield function to compression strength (left) and deviatoric plane (right)

The dynamic mechanical properties of concrete can be obtained by e.g., Hopkinson bar tests at different strain rates. The absence of dynamic experimental data for the C75 concrete necessitates using stain-rate sensitivity parameters from the literature. The data from the study by Polanco-Loria et al. [4] was used, i.e., $\dot{\varepsilon}_0 = 1.0 \cdot 10^{-5}$ and $C = 0.04$. Moreover, we ascertained the accuracy of the strain-rate sensitivity parameters with the experimental data from the CEB model code [9] and Magellanes et al. [10].

3.2 Setup of ballistic simulations

The setup is based on the numerical simulations from [5]. A 2D axisymmetric FE model was used for the with an element size of 1.0 mm (see Fig. 5). Hourglass type 6 was chosen with default values to prevent zero-energy deformation modes of the 4-node reduced integration volume weighted axisymmetric elements (element type 15). The elastic-plastic model **`*MAT_003`** with linear isotropic hardening was selected for the projectile. The material parameters of the projectile are Young's modulus $E_p = 200$ GPa, Poisson ratio $\nu_p = 0.3$, density $\rho_p = 7802$ kg/m3, yield stress $\sigma_y = 1720$ MPa and tangent modulus $E_{tan} = 15\,GPa$. Table 2 displays the material card of the MHJC model. Fig. 4 (right) shows the impact velocity versus the residual velocity points. The proposed calibration of the

MHJC parameters (given in Table 2) accurately predicts the residual velocities in the ballistic impact experiments, as shown in Fig. 4 (right).

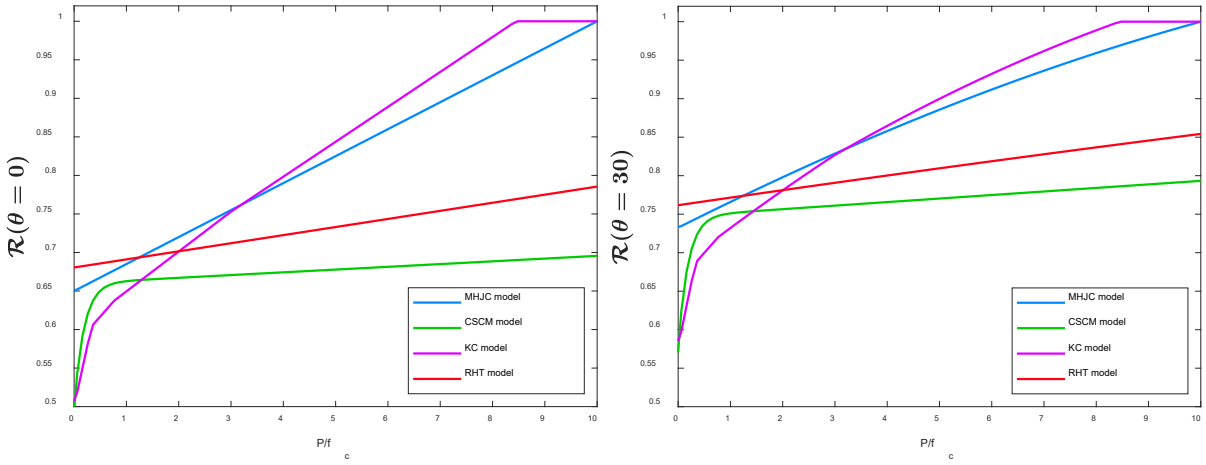

Fig. 3: Reduction factor of tension meridian (left) and shear meridian (right)

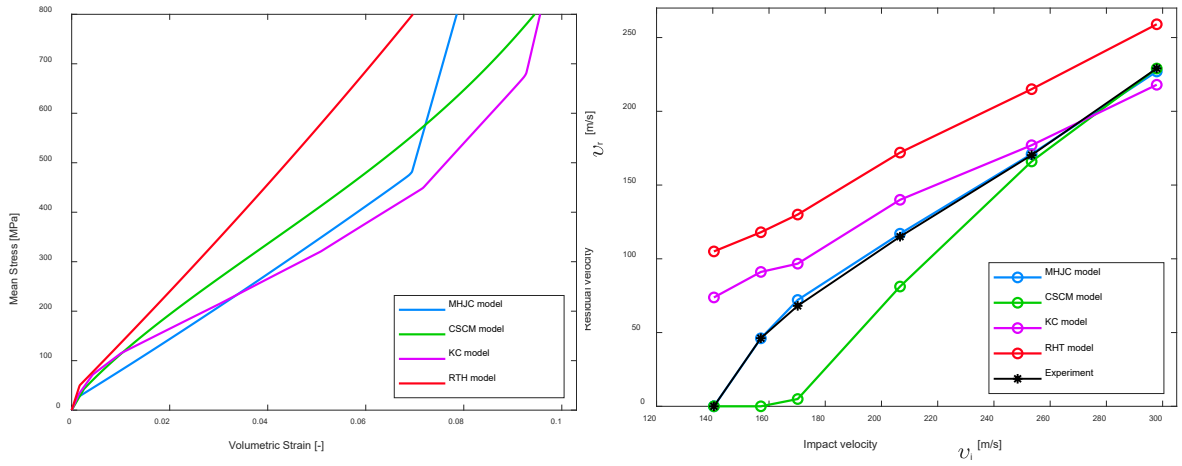

Fig. 4: Triaxial hydrostatic simulation (left) ballistic limit curves (right).

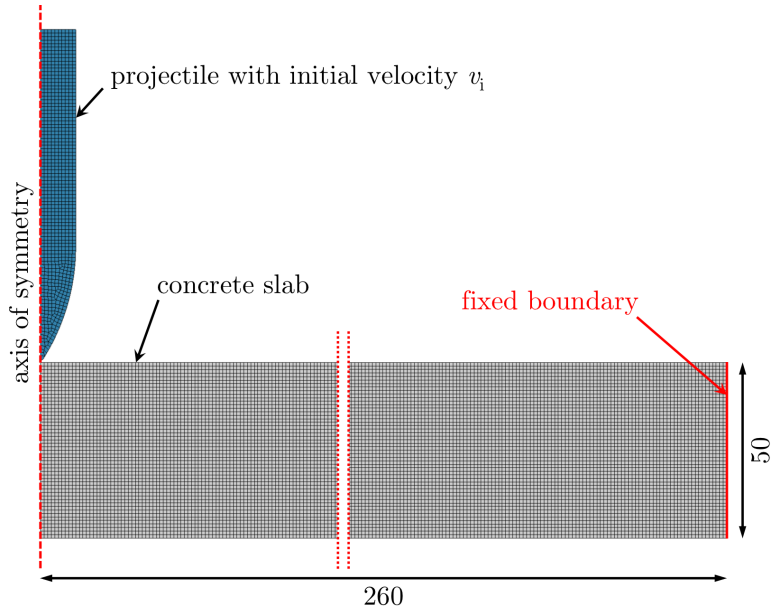

Fig. 5: 2D axisymmetric finite element model for ballistic impact tests [5].

3.3 Automatic parameter calibration option

The default parameter generation option determines the constitutive parameters of the models RHT, CSCM and K&C based on the cylinder compressive strength of the concrete. Their elastic response, compressive and tensile strengths are illustrated in Fig. 1. The CSCM model presents a lower stiffness compared with the experiment, while the RHT and K&C models give higher stiffness. In general, the compression test is quite good for all models and they capture the compressive peak stress well, while the K&C model gives the most accurate peak stress in tension. These results are encouraging given that only one mechanical material parameter is given to the models.

Comparing the yield surface of all the three models to the one from the MHJC in Fig. 2, we observe that at pressures under the uniaxial compression, the yield limit of the three models differs from the calibrated MHJC model. The yield surface of the K&C model differs notably for all pressures. However, at higher pressures, the yield surface of the CSCM model raises significantly, and the RHT model is slightly increasing. There is no coherence between the deviator planes of all the models. Additionally, the reduction factor of the tension and shear meridians in Fig. 3 appears considerably smaller for the RHT and CSCM models at high pressures. The reduction factors of the K&C and MJHC models are relatively close. It is worth mentioning that the reduction factor of the K&C model is computed internally. In contrast, constitutive equations control the reduction factors for the RHT and CSCM models.

The hydrostatic response in Fig. 4 (left) of the models CSCM, K&C and MHJC are reasonably similar until the solidification pressure limit ($P_l = 500$ MPa) of the MHJC model. After that point, the K&C model retains a smaller bulk modulus until approximately 600 MPa, where the solidification phase seems to initiate, and the slope becomes the same as the MHJC model. The solidification phase does not arrive for CSCM for the ranges of pressures calculated. However, the slope of the compaction phase seems to be increasing, leading to the third phase at a higher pressure. The RHT model overestimates the compaction phase of the pore evolution under hydrostatic pressure compared with the MHJC model, without any indication of initiating the solidification phase.

The broad diversity of the performance of the models in the material simulations implies different ballistic responses as plotted in Fig. 4 (right). Based on the automatically generated parameters, the RHT model predicts the lower perforation resistance and is thus overly conservative. Despite the accuracy of the CSCM model for impact velocities at 250 m/s and above, it overrates the perforation resistance for lower impact velocities. The K&C model reveals a tendency to reliably predict the residual velocity for impact velocities above 160 m/s. For the lower impact velocities, the K&C model is too conservative. As already pointed out, the calibrated MHJC model provides good correspondence with the experimental data. Thus, there is no reason to believe that given a proper calibration, the CSCM, RHT and K&C models should also be able to accurately predict the residual velocities.

*MAT_USER_DEFINED_MATERIAL_MODELS							
$# mid	rho	mt	lmc	nhv	iortho	ibulk	ig
1	2.47E-9	42	24	25	0	19	1
$# ivect	ifail	itherm	ihyper	ieos	lmca		
1	1	0	0	0	0		
$# G	A	Bc	C	Nc	fc	ft	K0
17.5E3	1.0	1.62	0.04	0.50	75.0	3.2	23.33E3
$# eps0dot	efmin	Smax	Pc	mu_c	Plock	mulock	
1.0E-5	0.01	7.0	25.0	1.071E-3	500.0	0.057714	
$# alpha	beta	K1	K2	K3	fs		
1.0	0.4	35.0E3	0.0	0.0	1.0		

Table 2: Material card of the MHJC model.

4 Summary and concluding remarks

In this study, the automatic parameter calibration options of the LS-DYNA concrete models RHT (***MAT_272**), CSCM (***MAT_159**) and K&C – Release III (***MAT_072R3**) were evaluated in terms of uniaxial compression, tension, triaxial hydrostatic compression, and ballistic impact experiments. The laboratory experiments were performed with a C75 high-strength concrete at SIMLab. The three models gave decent prediction for the cylinder compression test, while there was some divergence for tension and triaxial compression. The results of the ballistic impact simulations gave quite different

results depending on model, so one should be careful when using the parameter generator feature. Further, a modified version of the Holmquist-Johnson-Cook model (MHJC) was calibrated based on material tests and thus accurately predicted the ballistic impact experiments. There is therefore no reason to believe that the CSCM, RHT and K&C models would not give equally good results given a proper calibration. As a small case study, some parameters of the LS-DYNA concrete models were adjusted and thus more accurately represented the compression test as shown in Fig. 6 (left). Naturally, the tensile properties can also be adjusted like on the right in Fig. 6. A detailed calibration of these models is a laborious task and is hence left for further work.

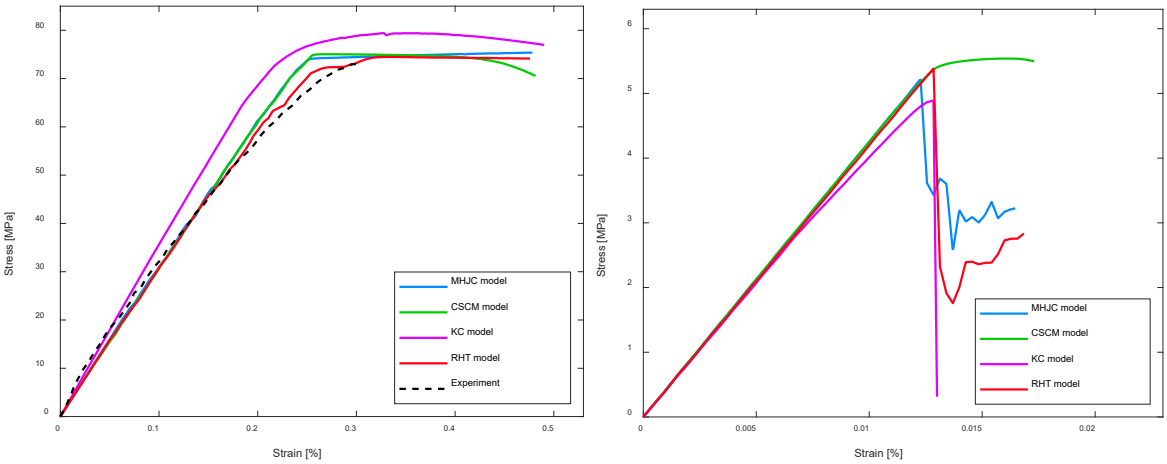

Fig. 6: Stress-strain curves of quasi-static compression (left) and tension (right)

5 Acknowledgements

The present work has been carried out with financial support from the Centre of Advanced Structural Analysis (CASA), Centre for Research-based Innovation, at the Norwegian University of Science and Technology (NTNU) and the Research Council of Norway through project no. 237885 (CASA).

6 Literature

[1] Grunwald, C., Schaufelberger, B., Stolz, A., Riedel, W., & Borrvall, T. (2017). A general concrete model in hydrocodes: Verification and validation of the Riedel–Hiermaier–Thoma model in LS-DYNA. *International Journal of Protective Structures, 8*, pp. 58-85.

[2] Murray, Y. (2007). *Users Manual for LS-DYNA Concrete Material Model 159.* Federal Highway Administration, publication no. FHWA-HRT-05-062.

[3] Malvar, L. J., Crawford, J. E., Wesevich, J. W., & Simons, D. (1997). A plasticity concrete material model for DYNA3D. *International journal of impact engineering*, *19*(9-10), 847-873.

[4] Polanco-Loria, M., Hopperstad, O., Børvik, T., & Berstad, T. (2008). Numerical predictions of ballistic limits for concrete slabs using a modfified version of the HJC concrete model. *International Journal of Impact Engineering, 35*, pp. 290-303.

[5] Kristoffersen, M., Toreskås, O. L., Dey, S., & Børvik, T. (2021). Ballistic perforation resistance of thin concrete slabs impacted by ogive-nose steel projectiles. *International Journal of Impact Engineering*, *156*, 103957.

[6] Malecot, Y., Daudeville, L., Dupray, F., Poinard, C., & Buzaud, E. (2010). Strength and damage of concrete under high triaxial loading. *European Journal of Environmental and Civil Engineering*, *14*(6-7), 777-803.

[7] Rubin, M. B. (1991). Simple, convenient isotropic failure surface. *Journal of engineering mechanics*, *117*(2), 348-369.

[8] Willam KJ, W. E. (1975). Constitutive model for the triaxial behaviourof concrete. *Proceedings of the International Assoc. for Bridge and Structural Engineering, vol. 19, pp. 1-30.* Bergamo, Italy.

[9] Comité Euro-International du Béton - Federation Interantional de la Precontraite. (1990). *CEB-FIP Model Code 90.* Trowbridge, Wiltshire, Great Britain: Redwood Books.

[10] Magellanes, J., Wu, Y., Malvar, L., & Crawford, J. (2010). Recent Improvements to Release III of the K&C Concrete Model. *11th Inernational LS-DYNA Users Conference, Dearborn, MI, A.US*.